Effect of Ambient Temperature and Discharge Current on Thermo-Electrochemical Behaviour of Lithium-Ion Cells Using Surrogate Modelling and Analysis

Journal of The Electrochemical Society, 2023 **170** 060526
1945-7111/2023/170(6)/060526/12/$40.00 © 2023 The Electrochemical Society ("ECS"). Published on behalf of ECS by IOP Publishing Limited

Effect of Ambient Temperature and Discharge Current on Thermo-Electrochemical Behaviour of Lithium-Ion Cells Using Surrogate Modelling and Analysis

Raghvendra Gupta, Supreet Singh Bahga, and Amit Gupta[z]

Department of Mechanical Engineering, Indian Institute of Technology Delhi, Hauz Khas, New Delhi, 110016, India

The thermal behaviour of lithium-ion cells plays a critical role in their overall performance and safety. The cell temperature fluctuates during operation due to varying operating conditions, particularly discharge current and ambient temperature. Thus, a precise thermo-electrochemical characterization is imperative for comprehending the behaviour of these cells under a wide range of operating conditions. Through experimental measurements, this study endeavours to determine the dependence of the thermo-electrochemical response of commercial lithium-ion cells as a function of discharge rates and ambient temperatures. High-fidelity reduced-order models are established using surrogate-based techniques to formulate response surfaces for the relevant output parameters, which enables the estimation of these parameters in cases where experiments were not performed. The study reaffirms that an increase in the discharge current rate results in an increase in the temperature difference between the core and surface of the cell. Also, a low ambient temperature has a relatively higher adverse impact on the battery performance, given the same discharge current. Furthermore, sensitivity analysis reveals that cell temperature, discharge capacity, and average discharge energy are more sensitive to ambient temperature than discharge current. On the other hand, the average discharge power is insensitive to ambient temperature and primarily dependent on the discharge current.
 [DOI: 10.1149/1945-7111/acd965]

Manuscript submitted March 17, 2023; revised manuscript received May 12, 2023. Published June 19, 2023.

List of Symbols

$\bar{E}_{dch}$	time-averaged discharge energy of cell (Wh)
$\bar{P}_{dch}$	time-averaged discharge power of cell (W)
$\bar{T}_s$	time-averaged surface temperature of cell (°C)
$\bar{T}_{core}$	time-averaged core temperature of cell (°C)
E_{dch}	discharge energy (Wh)
P_{dch}	discharge power (W)
Q_{dch}	discharge capacity (Ah)
T_{core}	core temperature of the cell (°C)
T_s	surface temperature of the cell (°C)
C-rate	current rate
DDM	data driven modelling
DOE	design of experiments
EIS	electrochemical impedance spectroscopy
LAM	loss of active material
LHS	latin hypercube sampling
LIBs	lithium-ion batteries
LLI	loss of lithium inventory
MSI	main sensitivity analysis
PP	polypropylene
PRESS	prediction error sum of squares
ROM	reduced order modelling
TPE	training point error
TSI	total sensitivity analysis

Lithium-ion batteries (LIBs) are currently the most popular type of energy storage technology due to their high volumetric and gravimetric energy densities,[1–3] low self-discharge[4,5] and long operational life.[6] LIBs have widespread applications in electronic devices (mobile phones, tablets, laptops and smartwatches), electric vehicles (EVs),[7] and grid energy storage systems.[8] The performance and safety of these battery technologies are directly affected by operating conditions such as discharge rate (C-rate) and ambient temperature.[9–12] The high-temperature environment acts as a catalyst and increases the side reaction kinetics. The increased side reactions result in the growth of the SEI layer, increase in internal resistance, loss of lithium inventory (LLI)[13–16] and dissolution of metal from the cathode.[13,17] The electrolyte starts to decompose over and above the temperature of 130 °C,[18] resulting in the loss of active material (LAM).[5] The polypropylene (PP) separators start to shrink above 150 °C,[19] which results in direct contact between anode and cathode, creating a short circuit and triggering thermal runaway.[20,21] On the other hand, a low-temperature environment slows the lithium-ion transport in the electrolyte, leading to lithium plating at a high charging rate due to lithium-ions crowding near the negative electrode side and causing loss of lithium inventory.[4] Further, continuous charging at high C-rates and low ambient temperature (below 15 °C) can cause dendrite formation, which penetrates the separator and results in short-circuiting of the cell.[22] High charge and discharge rates without constant voltage charging can result in localized overcharge and over-discharge,[23] which can result in the degradation of cells. Also, at a high C-rate (1C, 2C or more, depending upon the cell chemistry), the rate of side reactions increases, which accelerates the ageing of these cells.[24]

The core and surface temperature of a lithium-ion cell is not the same due to the different thermal conductivities of individual cell components. The thermal resistance of each lithium-ion cell component is very high, leading to a high-temperature gradient between the core and surface of these cells,[25,26] with the temperature gradient changing with a change in the operating conditions. The current rate and ambient temperature have been regarded to be the two major factors that have the most effect on the thermo-electrochemical performance of these cells.[27] Various researchers have conducted studies to understand the thermal response of the cells. Morali[28] performed thermal simulations to gain insights into the thermal dynamics of cells. In their simulations, the discharge current varied from 1C–3C rates, while the ambient temperatures were maintained at 15 °C, 25 °C, 35 °C and 45 °C. Morali[28] calculated the cell's convective heat transfer coefficient and state-of-health (SOH) using a multi-scale multi-dimensional modelling technique. Also, it was reported that the discharge current has a major role in the rise in temperature of the cell, and the SOH is the least contributor to the rise in temperature compared to other considered design parameters. Saxena et al.[27] studied the effect of different parameters such as charge current cutoff, discharge current rate, depth of discharge, ambient temperature and the combined effect of these parameters in the stress factor ranking of the cells using the data-driven modelling techniques. They reported that the individual and combined effect of

[z]E-mail: agupta@mech.iitd.ac.in

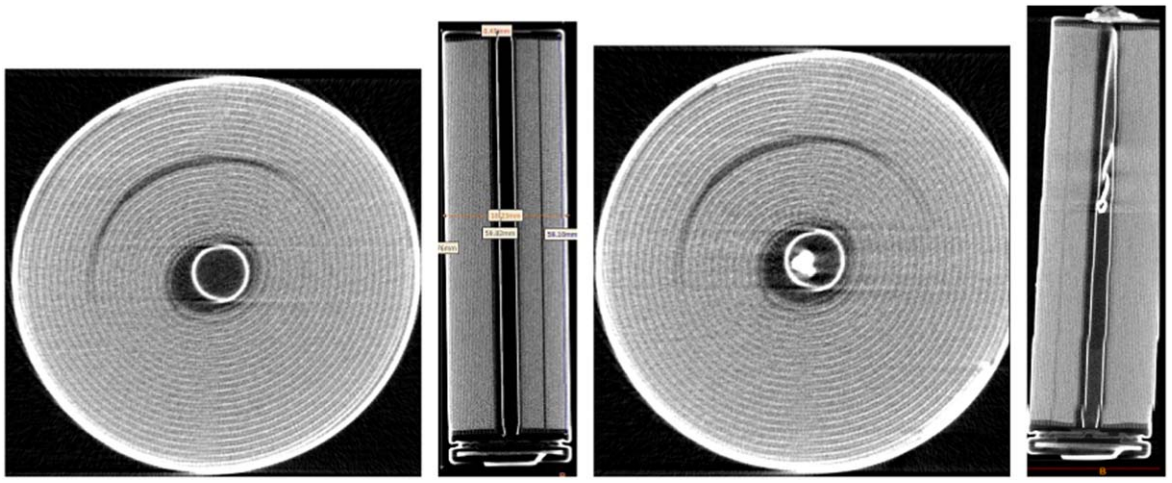

Figure 1. CT scan image of an unprobed cell from (a) top and (b) front, and probed cell from (c) top (d) front.

discharge current and ambient temperature causes maximum stress on the cell capacity compared to other reported stress factors. Similarly, Chang et al.[29] experimented on prismatic cells with a rated capacity of 50 Ah. The cell temperature distribution over the surface was recorded under different operating conditions. The discharge current ranged from 0.5C to 2C rate, and the climate conditions varied from −20 °C to 35 °C. Chang et al.[29] reported that the maximum temperature rise at −20 °C is 8.8 times higher compared to 35 °C ambient temperature. Similarly, different research groups[30–34] have investigated the impact of climate temperature and discharge current on the performance of lithium-ion batteries. However, the scope of these studies is limited to narrow operating conditions, which does not allow for exploration across a broad range of operating conditions for the Indian sub-continent, ranging from 0 °C to 45 °C and discharge rates of 0.5C to 3C. Moreover, the range anxiety issue for electric vehicle riders is a significant concern that can be addressed by providing an informed battery management system based on a trained reduced-order model that is used to estimate the internal temperature of a cell. Therefore, our study is focused on addressing this issue while also exploring a more comprehensive range of operating conditions than previous works.

The main objective of this study is to conduct a comprehensive analysis of the impact of ambient temperature and discharge current on the thermo-electrochemical performance of lithium-ion cells. In order to achieve this objective, a surrogate modelling technique was employed to estimate key output parameters, including core temperature, surface temperature, discharge capacity, average discharge

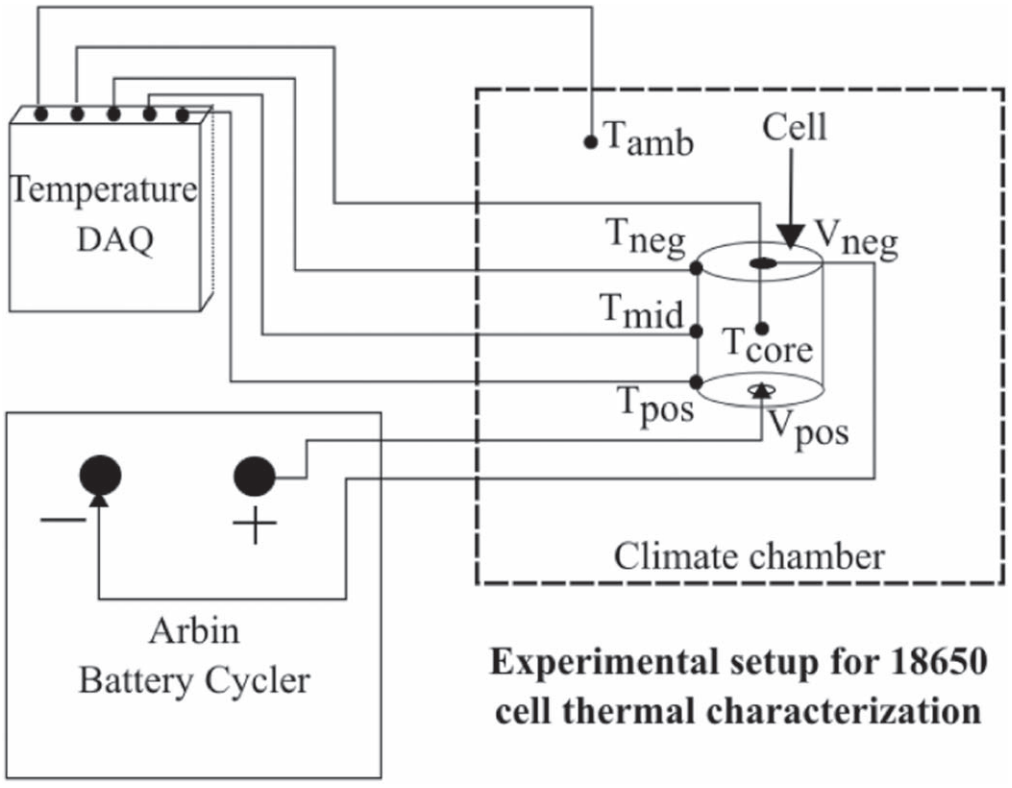

Figure 2. Experimental setup for thermal characterization of LIBs.

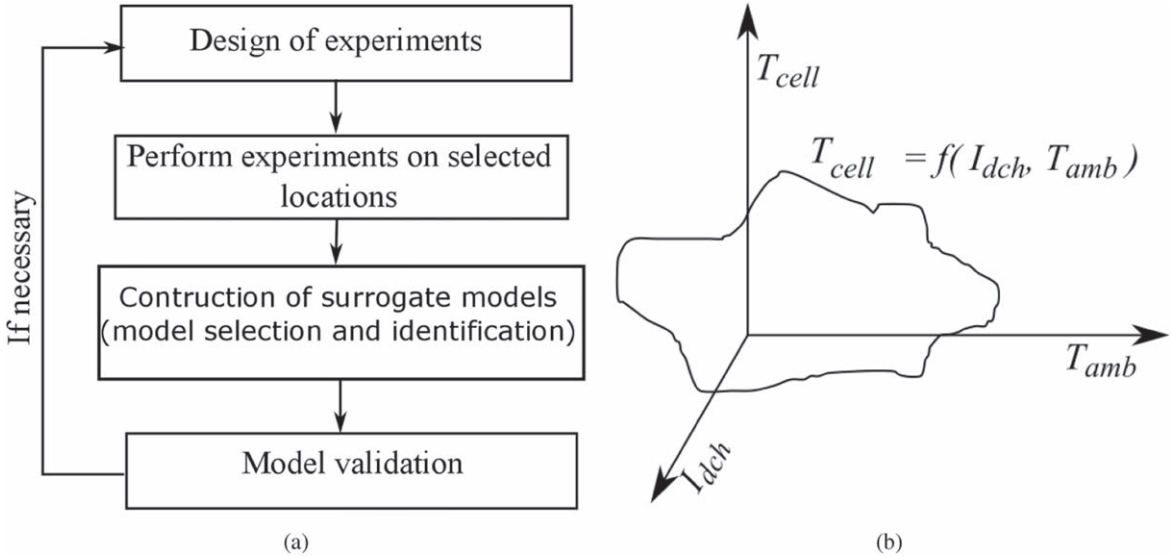

Figure 3. Surrogate modelling (a) flowchart and (b) an illustration of a fitted response surface as a function of design variables.

power, and average discharge energy. The manuscript is divided into several sections, with the Methodology section outlining the methodology, including details on the experimental setup, design of experiments, and surrogate modelling. The results and discussion section presents the results and discussions related to the thermo-electrochemical performance of commercial cylindrical cells, while the Conclusions section summarizes the conclusions and future work.

Methodology

The thermo-electrochemical characterization of lithium-ion batteries can be performed utilizing thermo-electrochemical (physics-based)[35,36] modelling or data-driven modelling techniques (DDM).[33,34,37] Physics-based models simulate the behaviour using governing equations based on the conservation of species and charge in the cell. These mathematical equations contain various internal parameters, including charge concentration in anode and cathode, particle radius, transference number, and ionic and thermal conductivity of electrolytes and electrodes, which are difficult to measure for commercial cells. To mitigate this burden, the application of the design of experiments in conjunction with data-driven modelling (DDM) techniques can be employed. These data-driven modelling (DDM) techniques, also called as reduced-order modelling (ROM), do not require mathematical equations and internal parameters, hence avoiding the challenges faced by physics-based modelling. Various reduced-order modelling techniques are reported in the literature, such as emulation, meta-modelling, approximate dynamic programming, artificial neural networks, and surrogate modelling. Among these, surrogate modelling is the simplest to implement as it is a high-fidelity statistical modelling technique requiring a small number of training and test data points in comparison to other machine learning approaches.[38–40] Hence, we employ surrogate modelling to develop models for the thermo-electrochemical response of a commercial lithium-ion cell.

Experimental setup.—Commercial 18650 lithium-ion Samsung cells with a rated capacity of 2.9 Ah have been used in this work to evaluate thermal behaviour and develop reduced-order models. The process begins by discharging the fresh cells to a cutoff voltage. Subsequently, a hole was drilled through the negative terminal of the cells in a controlled environment. A T-type thermocouple was carefully inserted along the axis of the cylindrical cell, and the hole was immediately sealed with marine weld paste. The cells were then placed in a controlled atmosphere for 12 h to ensure the marine weld was thoroughly cured. The proper contact of the inserted thermocouple with the core was verified using X-ray tomography, as shown in Fig. 1, which confirms that contact has been established successfully.

Table I. The range of input variables used in the experiments.

Input variables	Minimum	Maximum
Discharge current	0.5C	3C
Ambient temperature	0 °C	45 °C

The experimental setup used in the present study is shown in Fig. 2. An Arbin battery cycler having a configuration of 5 V and 60 A was used for the discharging processes. A constant ambient temperature was maintained using a Cincinnati sub-zero thermal chamber. The temperature of the cell was recorded with the help of a T-type thermocouple and National Instrument (NI) data acquisition system (DAQ) (NI9214 and chassis NI 9171). The NI DAQ was used to receive and process the signals. The surface temperature of the cells was measured at three locations, as shown in Fig. 2, the first near the positive terminal, the second at the mid-height of the cell's surface and the last near the negative terminal.

A standard protocol is followed to initially charge and rest the cell before starting the discharge process. It was observed that the cell acquires thermal equilibrium with the surroundings when left under OCP conditions for a duration of 2 h. Subsequently, the cells were charged at a constant current of 0.5C rate till the upper cutoff voltage was reached. Thereafter, the cells were charged at a constant voltage till the current dropped to 0.05C-rate. Further, the cell was discharged at different operating conditions of discharge rates and ambient temperature. This leads to the generation of heat and a rise in the cell temperature. Once the cell was completely discharged, the cell was allowed to cool down to ambient temperature by natural convection, which happens over a time scale of 30 m.

Design of experiments.—The design of experiments (DOE) technique was used to find conditions under which experiments are performed. The DOE also reduces the requirement of the total number of experiments[41,42] by incorporation of two techniques, namely central composite design (CCD) and Latin hypercube sampling (LHS)[43,44] to select the experimental parameters. The central composite design, also called Box and Wilson design, distributes the sample on the edges, centre of edges, and centre of the design space. The LHS is a restricted stratified sampling technique that distributes sample data points (say N_s) with an equal

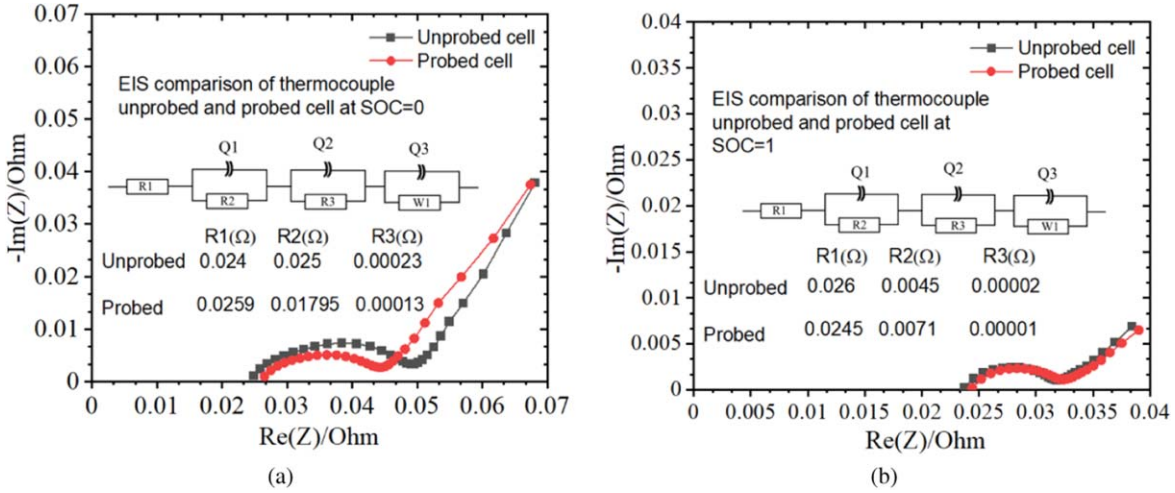

Figure 4. EIS curve comparison of probed and unprobed cells at (a) SoC = 0 and (b) SoC = 1.

marginal probability (of $1/N_s$). In LHS design, the samples can be distributed in different orders in terms of uniformity to achieve each dimension with equal sampling precision. This approach improves accuracy and reduces variance.[45] The experiments were performed on the selected experimental parameters, and the output data was fed to train a reduced-order model. The minimum and maximum values of input design variables are listed in Table I.

Initially, fitting reduced-order models was attempted with 20 DOE points, which were divided into two sub-groups of 18 training and 2 test data points. These data fed into the surrogate model resulted in PRESS and test point error of more that 10%. This indicates the insufficiency of training data points. Hence, the DOE was refined by adding more data points. Finally, a total of 40 data points were used as input for experiments, where 9 data points were selected using CCD, and the other 31 data points were selected using the LHS filling technique. The CCD technique distributes the data at 8 corners of the design space and the remaining 1 at its centre, while the LHS fills the remaining data points by maximizing the minimum distance among data points for distribution in the design space.

Surrogate modelling.—The flowchart shown in Fig. 3 represents the operational methodology of constructing a surrogate model. In the surrogate model, data points obtained from experiments are divided into training and test data sets. The training data sets are used to train the model, and after establishing the model, testing data sets are used to analyze the model's accuracy.[33] Various types of

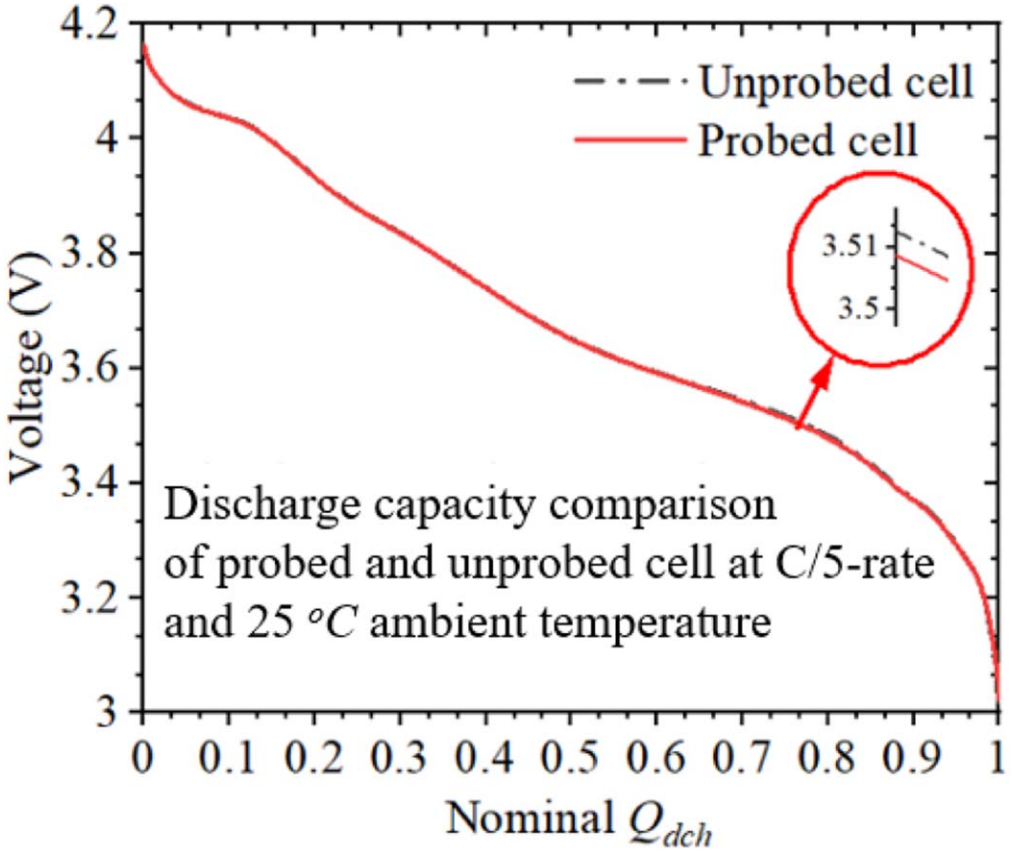

Figure 5. Fresh cell discharge capacity comparison of probed and unprobed cells.

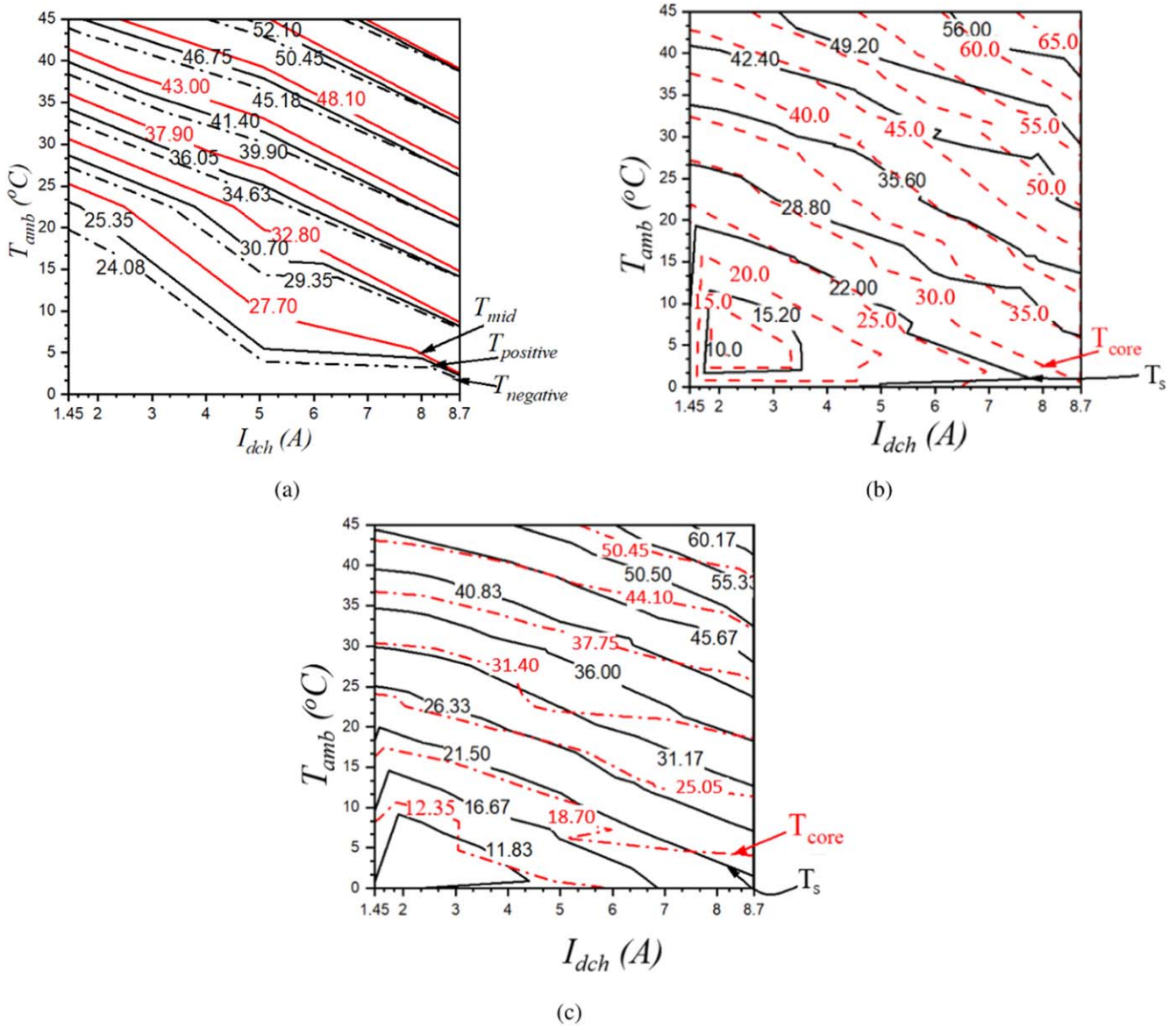

Figure 6. (a) Measured surface temperature comparison of the cell at three specified locations for nine CCD points, (b) maximum and (c) average core and surface temperature comparison at all DOE points.

Table II. The temperature rise of cells at different discharging C-rates when cells are covered with and without sleeves.

C-rate	Temperature rise with sleeves (°C)	Temperature rise without sleeves (°C)	ΔT (°C)
1-C	3.2	4.4	1.2
2-C	9.0	12.2	3.3
3-C	14.9	21.2	6.2
4-C	21.5	29.8	8.3

surrogate models are available, such as polynomial response surface model, kriging, support vector regression, and radial basis neural network.[46] The present study incorporated the Kriging model, also called as the Gaussian process regression. The Kriging model is capable of handling non-linear relationships between the input and output variables and measuring the prediction uncertainty, which is useful for decision-making due to its ability to provide unbiased and minimum variance estimates. The kriging technique employs a model that interpolates the underlying system's behaviour, as mentioned in Eqs. 1–5.[33,46]

$$\hat{y}(\mathbf{x}) = z(\mathbf{x}) + \sum_{i=1}^{n} \beta_i f_i(\mathbf{x}), \quad [1]$$

where n was the number of measurements data points, β_i were the weights assigned to each observed output $f_i(\mathbf{x})$ and $z(\mathbf{x})$ was the residual term, which was described as a realization of a stochastic process $Z(\mathbf{x})$ with mean zero, process variance σ^2, and covariance function given by

$$\mathrm{cov}(Z(\mathbf{x}_i), Z(\mathbf{x}_j)) = \sigma^2 R(\mathbf{x}_i, \mathbf{x}_j), \quad [2]$$

where $R(\mathbf{x}_i, \mathbf{x}_j)$ is the correlation between $\mathbf{x}_i$ and $\mathbf{x}_j$, The weights are determined using a Gaussian covariance function:

$$\beta_i = \frac{1}{\sum_{j=1}^{n} \lambda(\mathbf{x}_j)} \lambda(\mathbf{x}_i), \quad [3]$$

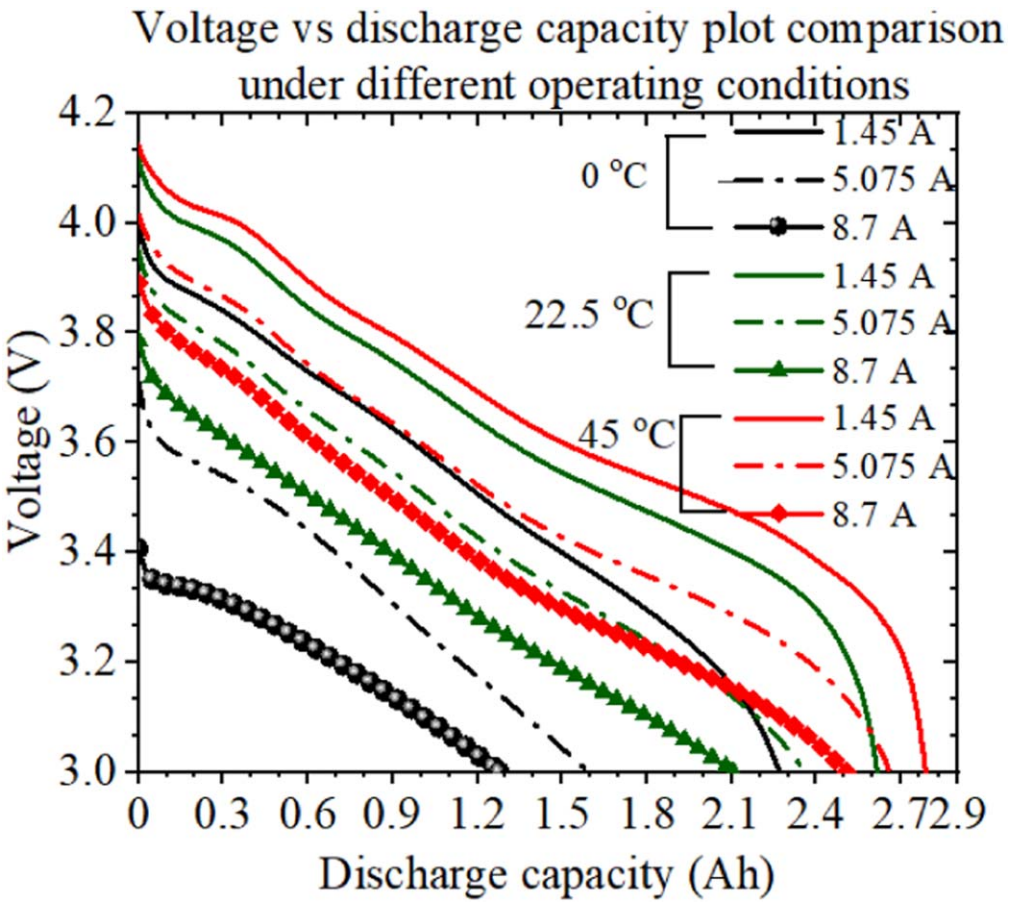

Figure 7. Voltage vs discharge capacity for nine CCD points.

where $\lambda(\mathbf{x}_i)$ is the Gaussian kernel between the observed data point at location $\mathbf{x}_i$ and the estimated point at location $\mathbf{x}$:

$$\lambda(\mathbf{x}_i, \mathbf{x}_j) = \sigma^2 \exp\left(-\frac{1}{2}\sum_{d=1}^{D}\left(\frac{x_{id} - x_{jd}}{\ell_d}\right)^2\right), \quad [4]$$

where ℓ_d is the length scale of the dth predictor, and D is the number of predictors. In this case, the length scale ℓ_d controls the smoothness of the function in the dth dimension.

$$Z(x) = z(x) - \varphi(x)\alpha, \quad [5]$$

The kernel function $\lambda(\mathbf{x}_i, \mathbf{x}_j)$, constant basis ($\phi(x)$), and estimated coefficient of the constant basis α, β and σ are the different coefficients used for model fitting. The kernel function is a mathematical function that describes the correlation between the input variables. The choice of the kernel function directly impacts the model accuracy. In the current study, the squared exponential kernel function is considered. The basis function encapsulates the functional characteristics utilized for constructing the model.[46] The kriging weight (β) is an assigned weight corresponding to each observed output in the model. The process variance, σ^2, quantifies the variability of the modelled data. The error quantification was done by a technique known as prediction error sum of squares (PRESS), which uses only the training data set to evaluate the model by employing the leave-one-out strategy to develop several new models and using the removed point as a test point to quantify error. The other technique that was incorporated into the modelling is the relative test point error. The formulae to calculate these errors are listed in the equations provided below.[33]

Prediction error sum of square (PRESS):

$$PRESS = \left(\sqrt{\frac{\sum_{i=1}^{n}(y_i - \hat{y}_i)^2}{n}}\right)\cdot 100, \quad [6]$$

Test point error:

$$TPE = \frac{(y_i - \hat{y}_i)}{y_i}\cdot 100, \quad [7]$$

Here, n is the number of sample data points, y_i is the output vector of ith data, and $\hat{y}_i$ is the estimated value from the surrogate model.

Sensitivity analysis.—Sensitivity analysis is a technique used to evaluate the impact of variations in input parameters on the measured outcome. The discharge current and ambient temperature are the two input parameters considered to affect the thermo-electrochemical response of a lithium-ion battery in different ways. One popular method for global sensitivity analysis is the Monte Carlo method, which is a probabilistic sensitivity analysis technique that generates random samples of the input variables from probability distributions and uses these samples to run and evaluate the model multiple times.[33] The standard main sensitivity indexes (MSI) include Sobol indexes, based on a variance-based index approach that quantifies the individual input variables with total output variance. On the other hand, total sensitivity indexes (TSI) take into account the interactions between the input variables and quantifies the input variables' overall effect on the model's output.

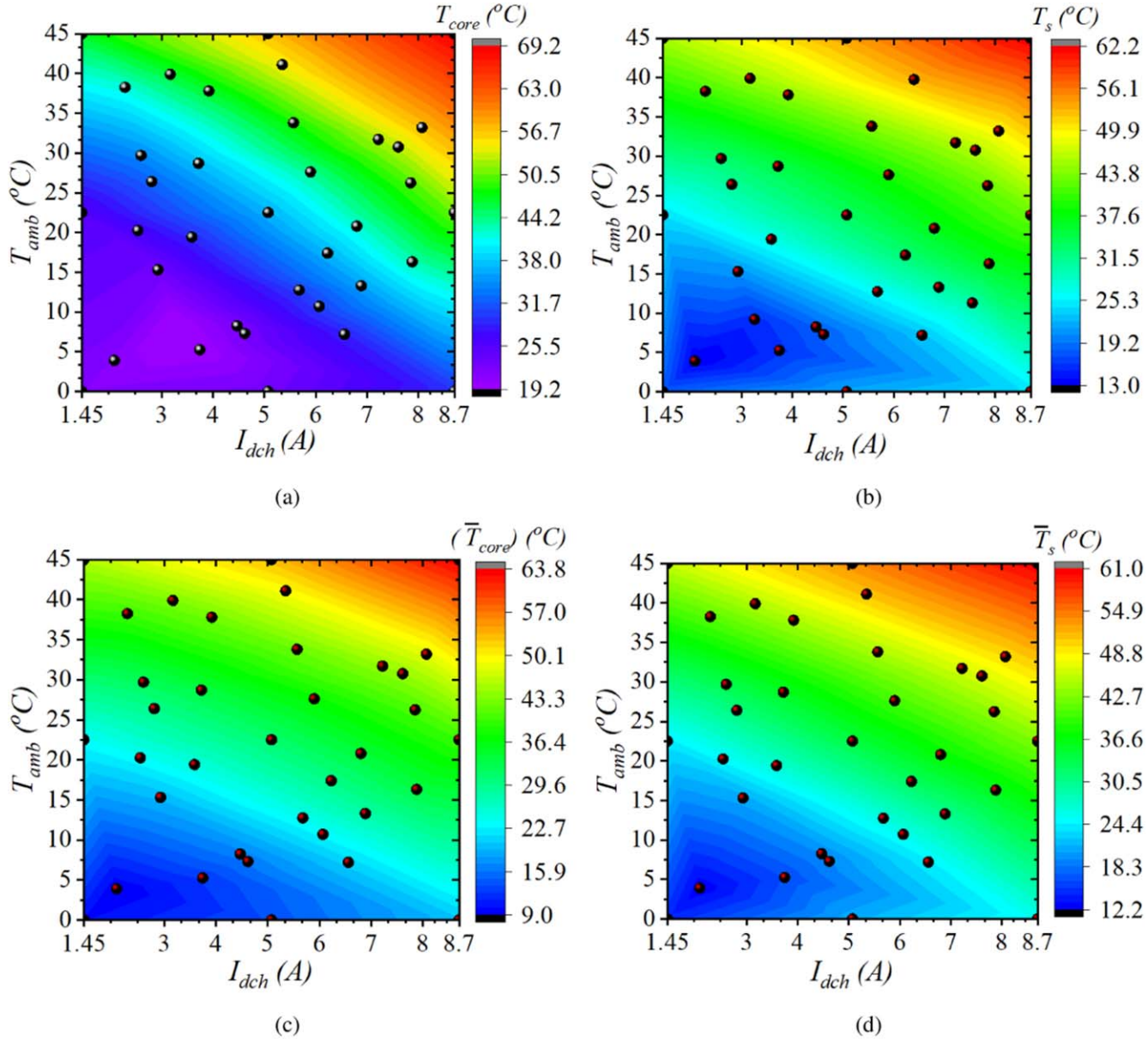

Figure 8. Contour plots of maximum (a) core temperature, (b) surface temperature, time-averaged (c) core temperature, and (d) surface temperature, and the symbols represent the DOE points where the experiments have been performed.

Methods for data analysis.—The temperature at the different locations was directly measured by the thermocouple interfaced with DAQ, whereas the other performance indicators, such as discharge capacity, average discharge power and average discharge energy, were calculated with the data recorded by the battery cycler containing data related to test time, current applied and voltage of the cell. The following formulae were used to calculate the performance variables.

Discharge capacity ($Q_{\max}$): The discharge capacity of the cell is calculated using the coulomb counting method as mentioned in the Eq. 8.

$$Q_{dch} = \int_{t_0}^{t_1} I(t)dt, \qquad [8]$$

where *I(t)* is the discharge current through the cell at time t and t_0 and t_1 are the start and end times of the discharge cycle, respectively.

Average discharge power ($\bar{P}_{dch}$): The average discharge power is calculated by the time averaging the total power obtained during the discharge cycle as,

$$\bar{P}_{dch} = \frac{1}{\Delta t}\int_{t_0}^{t_1} V(t)I(t)dt, \qquad [9]$$

where *V(t)* and *I(t)* are the instantaneous voltage and current, respectively, and $\Delta t = t_1 - t_0$ is the discharge time.

Average discharge energy ($\bar{E}_{dch}$): The average discharge energy of the lithium-in cells is calculated using time integral of average discharge power,

$$\bar{E}_{dch} = \bar{P}_{dch}\cdot\Delta t, \qquad [10]$$

where $\bar{P}_{dch}$ is the average discharge power, and Δt is the discharge time.

Sensitivity indexes calculation: The main sensitivity (MSI) and total sensitivity indexes (TSI) are calculated using the Sobol technique using the following formulae:

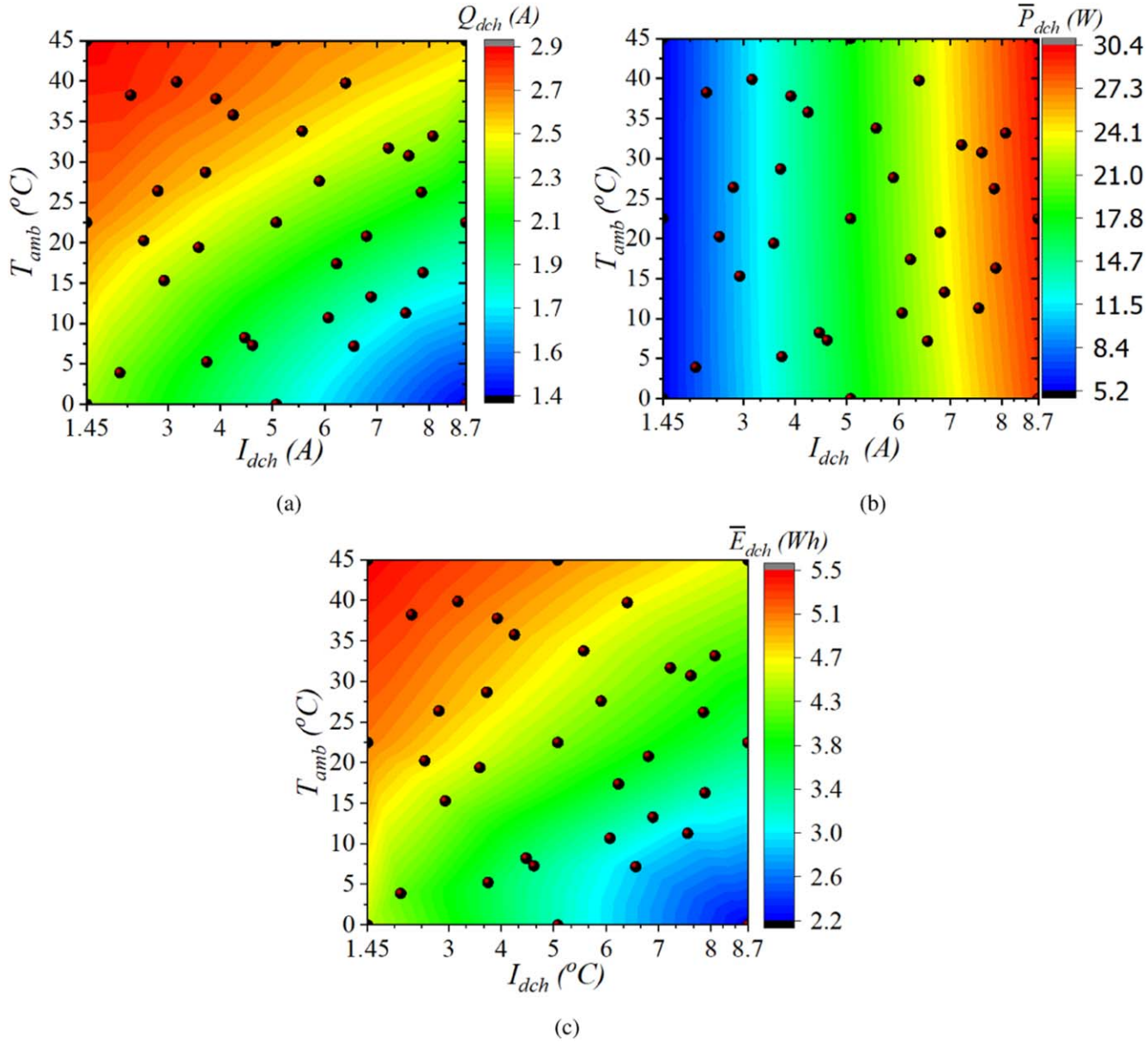

Figure 9. Contour plot of (a) maximum discharge capacity, time-averaged (b) discharge power and (c) discharge energy.

Main sensitivity indexes (MSI):

$$MSI_i = \frac{V_i}{V(Y)} \quad [11]$$

Total sensitivity indexes (TSI):

$$TSI_i = 1 - \sum_{j=1}^{j-1} S_j \quad [12]$$

where S_j was calculated using the equation provided below

$$S_j = \frac{V[\mathrm{E}(Y|X_i)]}{V(Y)} \quad [13]$$

Here, X_i is input variables, $V[\mathrm{E}(Y|X_i)]$ is the conditional variance of output variable, and $V(Y)$ is the total variance of output variable Y. S_j is the main sensitivity index associated with the first order Sobol indexes. V_i is the variance of the model output due to variations in the ith input variable.

Results and Discussion

Our analysis commenced with performing electrochemical impedance spectroscopy (EIS) of the probed and unprobed cells and their comparison at both fully discharged and charged states, as illustrated in Fig. 4. It can be observed from this figure that there is minimal variation in the cell's impedance, indicating that creating a deep hole in the core does not alter the thermo-electrochemical response of the cell. Additional experiments were carried out to evaluate variations in cell discharge capacity. It begins with the charging of both the probed and unprobed fresh cells. Firstly, these cells were maintained at 25 °C for 2 h and then charged at a constant current (CC) of 0.5C until the upper cutoff voltage of 4.2 V. The cells were then charged under constant voltage (CV) conditions until reaching a current cutoff of 0.05 C rate. After ensuring the full charge, the cell was discharged at a 1C rate till the lower cutoff voltage of 3 V. As illustrated in Fig. 5, the results indicate a negligible difference in the discharge capacity of these cells.

Most commercial cells are equipped with an outer insulation covering, which conveys information regarding the battery specifications. However, this insulation cover can influence the temperature

Table III. The maximum and minimum values of various thermo-electrochemical performance outcomes at different input design data points.

	$I_{dch}(A)$	T_{amb} (° C)	T_s (° C)	T_{core} (° C)
Min	0.5C	45	1.3	2.1
Max	3C	0	23.3	29.5
	$I_{dch}(A)$	T_{amb} (° C)	$Q_{dch}(Ah)$	
Min	3C	0	0.46Q	
Max	C/2	45	1Q	
	$I_{dch}(A)$	T_{amb} (° C)	$P_{dch}(W)$	
Min	C/2	0	5.1	
Max	3C	45	29.5	
	$I_{dch}(A)$	T_{amb} (° C)	E_{dch} (Wh)	
Min	3C	0	0.21E	
Max	1.45	45	0.51E	

Table IV. Parameters of the fitted kriging model.

Output variables	Kernel function	Basis	α	σ
T_{core}			48.96	0.81
T_s			30.66	1.55
$\bar{T}_{core}$			44.83	0.72
$\bar{T}_s$	Squared exponential	Constant	36.03	1.23
Q_{dch}			2.32	0.07
$\bar{P}_{dch}$			0.75	0.18
$\bar{E}_{dch}$			4.28	0.13

measurement on the cell's surface. Data from the experiments, as listed in Table II, indicate that as the discharge current increases, the rise in surface temperature difference between cells with and without sleeves increases (reference ambient temperature at 25 °C). This finding suggests that removing the sleeve will improve the cells' thermal characterization. So, all experiments in the present study were performed utilizing cells that had no sleeves.

Core and surface temperature measurement and estimation.— The core and surface temperature of cells are measured with the help of T-type thermocouples. One thermocouple was placed inside the cell's core, and three thermocouples were placed on the outer surface. The maximum temperature is recorded at the cell's core. Figure 6a shows that the surface temperature is maximum at the centre of the cell compared to the positive and negative terminals. As a result, the temperature at mid-height is considered for the surface temperature estimation. Three cells were used for each experiment, and the data was then averaged to minimize the measurement error. Figures 6b and 6c show the maximum and average measurement core and surface temperature comparison plots, respectively, for the chosen range of operating conditions. The average temperature refers to the time-averaged temperature of the complete discharge cycle. The voltage vs discharge capacity curve for the 9 CCD points is plotted as shown in Fig. 7. This figure illustrates that the ambient temperature and the discharge current both affect the electrochemical performance of the cell. Further experiments and analysis will be used to quantitatively analyze the effect of operating conditions on the thermo-electrochemical performance of the cells.

The contour plots in Figs. 8a and 8b depict the variation of measured maximum core and surface temperatures, respectively. On the other hand, Figs. 8c and 8d illustrate the average core and surface temperature variation, respectively. The factors associated with heat generation cause a temperature rise in cells. The primary contributors to heat generation are irreversible losses, entropic heat generation, and heat of mixing. Irreversible heat generation is a combination of various overpotentials, such as charge transfer overpotential, ohmic overpotential, and concentration overpotential. The ohmic overpotential and charge transfer overpotential increase at low temperatures due to low ionic and electronic conductivity, resulting in more irreversible heat than higher temperature counterparts for the same discharge rate. The contribution of reversible heat and heat of mixing becomes insignificant compared to irreversible heat at higher discharge rates. The maximum relative temperature rise with respect to ambient is recorded in the experiment at a 3C discharge rate and 0degC ambient temperature, which is approximately 5 °C higher than one obtained of the same discharge current and 45 °C ambient temperature. This is due to the higher overpotential of 0.8 V at 0 °C compared to 0.42 V at 45 ° C ambient temperature.

The relative PRESS and relative test point error (RTPE) for the estimation of core and surface temperature are bounded within 6.3% and 2.2%, respectively. The maximum rise in core and surface temperature was measured at approximately 29.5 °C and 23.5 °C, respectively. In contrast, the minimum rise in core and surface temperature was 2 °C and 1.3 °C, respectively. The average core and surface temperature represent the average rise in the cell temperature over the complete cycle. The maximum relative PRESS and RTPE are 7.1% and 3.3% for estimating the cell's average core and surface temperature, respectively. The maximum average core and surface temperature are estimated as 63.8 °C and 61 °C, respectively.

Discharge capacity estimation.—Discharge capacity (Q_{dch}) is calculated using the coulomb counting method as given in Eq. 8. A corresponding contour plot relates the discharge capacity with the discharge current and ambient temperature. The plot shown in Fig. 9a represents the variation in the discharge capacity obtained by fitting a kriging model. The relative PRESS and relative test point error for the estimation of Q_{dch} are calculated as 4.8% and 3.3%, respectively. The maximum Q_{dch} for particular input conditions is calculated as 100% of the nominal capacity of the cell, while the minimum is estimated as 46%.

The discharge capacity of a cylindrical 18650 cell is a function of various factors, including discharge current and ambient temperature. The cell's internal resistance is the primary factor affecting the discharge capacity, which increases with a higher discharge current and decreasing ambient temperature. The increase in internal resistance reduces the amount of energy that can be delivered to the load, thereby decreasing the discharge capacity of the cell. Moreover, when the discharge current is high, and the ambient temperature is low, a relatively higher proportion of energy is lost as heat, which further reduces the discharge capacity of the cell. Furthermore, at lower ambient temperatures, the electrolyte in the cell becomes highly viscous. The increase in viscosity manifests as a lower diffusion coefficient in the electrolyte phase, resulting in transport limitations due to the increase in electrolyte resistance. This limits the movement of ions, further reducing the discharge capacity of the cell. Therefore, the discharge capacity of a cylindrical 18650 cell is a complex function of various factors, including discharge currents, ambient temperature, and internal resistance, which must be considered when designing or using such cells.

Average discharge power estimation.—The average discharge power is calculated by time-averaging the product of the applied discharge current and the instantaneous voltage (see Eq. 9). The overpotential of the cell increases when it is operated under a high current, leading to a power loss. Additionally, an increase in overpotential occurs during the low-temperature operation of the cell, which results in a loss of power within a given cycle. It is observed that the average discharge power has a strong influence on the discharge current but is relatively insensitive to climate conditions. This is clear from the contour plot of the reduced-order model shown in Fig. 9b. The goodness of the fitted kriging model fitting is

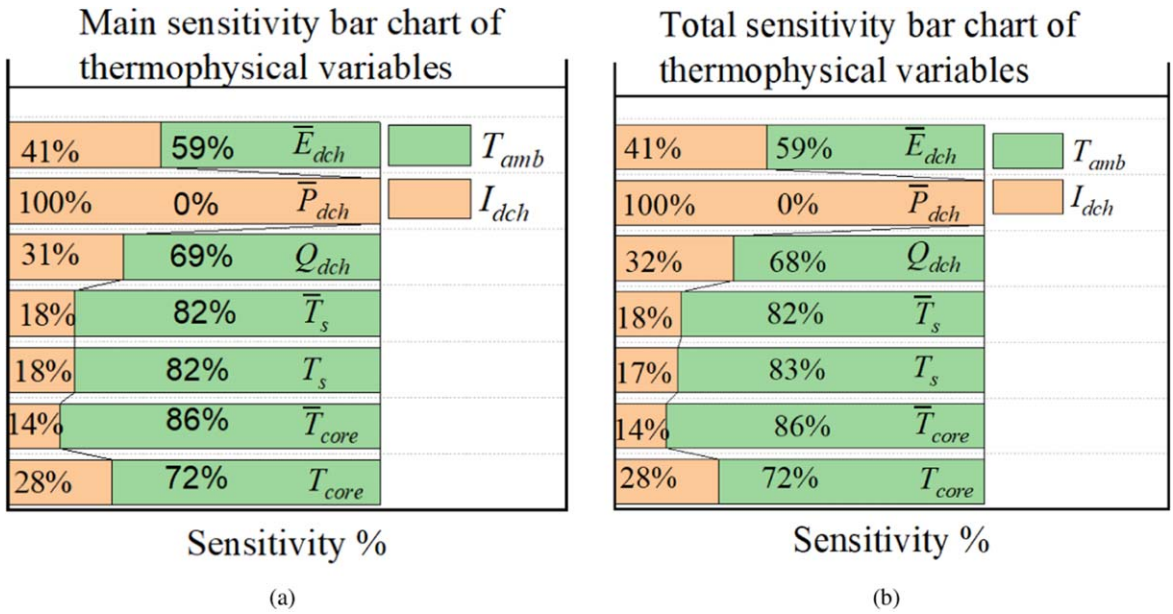

Figure 10. Sensitivity bar chart for thermo-electrochemical variables showing (a) main sensitivity and (b) total sensitivity.

quantified by the relative PRESS and relative test point error of estimation, which are 1.18% and 0.06%, respectively.

Average discharge energy estimation.—The discharge energy of LIBs is a measure of the energy released during the electrochemical redox reaction that occurs during the discharge process. This discharge energy is calculated as the product of the discharge capacity and the average discharge voltage of the battery (see Eq. 10). The discharge energy is directly influenced by the discharge capacity for fixed upper and lower cutoff voltages, which in turn is affected by various parameters, including the discharge current and ambient temperature. The relationship between the discharge energy and these parameters is nonlinear, as can be seen in the variation of the discharge energy at high C-rates and low ambient temperatures. As shown in Fig. 9c, this relationship can be further explored through a contour plot, which represents the overall variation of discharge energy in response to changes in input variables. The low relative PRESS and relative test point errors demonstrate the accuracy of this model. These errors are calculated as 3.92% and 0.03%, respectively, which indicates that the model is accurate and can be relied upon to accurately predict the discharge energy of lithium-ion batteries under various operating conditions.

Table III presents the maximum and minimum values of thermo-physical variables corresponding to a provided range of input variables. An analysis of the data in this table indicates that the maximum temperature increase is observed when discharging the battery at a 3C discharge rate and an ambient temperature of 0 °C. This observation contrasts with the expectation that a higher ambient temperature of 45 °C would result in a significant temperature rise. This phenomenon can be explained by the higher ionic resistance of the liquid electrolyte medium in LIBs at low ambient temperatures. The increased internal resistance results in more significant heat generation within the battery, leading to a rise in temperature during discharge. Moreover, the results reveal that the discharge capacity and average discharge energy are minimum when the battery is discharged at a 3C rate and under a 0 °C ambient temperature. This finding aligns with the inverse relationship between discharge capacity, discharge rate, and the decrease in discharge energy at low temperatures. Therefore, these results suggest that the choice of discharge rate and ambient temperature can significantly impact the thermo-physical performance of lithium-ion cells and that these factors must be carefully considered when designing and operating these cells.

The parameters of the fitted kriging model are tabulated in Table IV, corresponding to each output variable. The constant basis function is important in kriging because it allows for the model to capture any global trends or biases in the data, in addition to the local spatial correlation captured by the random process.[47]

Sensitivity analysis.—The accuracy of the estimation is contingent upon the measurement accuracy and the sensitivity of the input parameters. It has been observed that different output variables, such as core temperature (T_c), surface temperature (T_s), discharge capacity Q_{dch}, average discharge power P_{dch}, and average discharge energy E_{dch}, exhibit varying levels of sensitivity to the input variables. Sensitivity analysis has been performed using Monte Carlo global sensitivity analysis to gain a deeper understanding of this variation. 10^6 Monte Carlo simulation points were used to calculate the input variables' main and total effects.

The relative impact of climate conditions and discharge currents on the thermo-physical response of lithium-ion batteries was investigated using sensitivity analysis. Figure 10 indicates that a change in ambient temperature has a more significant impact on the core and surface temperature of the cell than the variation in discharge current. Temperature affects the chemical reactions within the battery cells, with increased temperature accelerating the reaction kinetics, leading to higher heat generation and temperature rise. However, the sensitivity of the surface temperature to ambient temperature and discharge current is different from the sensitivity of the core temperature. The heat generated within the cell primarily dissipates through the surface and depends on the convective heat transfer coefficient and the temperature difference between the cell and the environment. In addition, the discharge capacity is influenced by both ambient temperature and discharge current. The increase in discharge current leads to higher overpotential and more energy loss in the form of irreversible heat, which decreases the discharge capacity. As shown in Fig. 10, the discharge capacity is more sensitive to changes in ambient temperature than the discharge current. On the other hand, the average discharge power of the cell is mainly determined by the discharge current, with minimal impact from ambient temperature changes. The energy released from the cells is primarily determined by the rate of chemical reactions within the cell, which is mainly controlled by the discharge current. The discharge energy, which is related to the discharge capacity and voltage, is more sensitive to changes in the discharge current than to changes in the ambient temperature.

Conclusions

In this study, commercially available 18650-type commercial cells with a nominal capacity of 2.9 Ah were utilized to investigate the thermo-electrochemical behaviour of lithium-ion cells for a broad range of operating conditions that typically prevail in the Indian subcontinent. The results indicate that the relative increase in core and surface temperature is higher at low temperatures (below 15 °C) compared to higher temperatures for the same discharge rate. This is due to an increase in the viscosity of the liquid electrolyte at low temperatures, which causes an increase in resistance to the motion of lithium ions and results in a high irreversible heat generation. The maximum overpotential in this study was determined to be 0.8 V at a 3C discharge rate and 0 °C ambient temperature. Additionally, the maximum relative rise in core temperature (29.5 °C) with respect to ambient was also observed under these conditions. The discharge capacity of the cells for a given discharge current increases with an increase in the ambient temperature. The average discharge power is solely a function of the discharge current. The maximum average discharge power was measured to be 29.5W at a 3C discharge rate and 25 °C ambient temperature. It is worth noting that the average discharge power was the same for constant 3C-rate and ambient temperatures of 0 °C, 22.5 °C and 45 °C, indicating that the discharge power is insensitive to ambient temperatures and only dependent on the discharge current. Similarly, the average discharge energy was maximum at low discharge current and higher ambient temperatures due to increased reaction kinetics. The average discharge energy was sensitive to both the discharge current and the ambient temperature but relatively more sensitive to the latter.

In all the experiments presented in this work, the heat transfer from the cell under discharge conditions occurred by natural convection. The analysis could also be extended to forced cooling conditions, which will render the results suitable for designing a cooling system for a battery pack. This study will be presented in the future. Also, the outcome of this study could be used as a guideline for developing BMS and cooling systems for similar commercial cells.

Acknowledgements

This work was partially supported by the Department of Science & Technology, Government of India, under the Energy Storage Platform on Batteries (ESPOB). The support from ReNew Power is also gratefully acknowledged.

ORCID

Raghvendra Gupta https://orcid.org/0000-0001-9496-1731
Amit Gupta https://orcid.org/0000-0001-6709-7095

References

1. M. Rashid and A. Gupta, "Mathematical model for combined effect of sei formation and gas evolution in li-ion batteries." *ECS Electrochem. Lett.*, **3**, A95 (2014).
2. J. Tarascon and M. Armand, "Issues and challenges facing rechargeable lithium batteries." *Nature*, **414**, 359 (2001).
3. N. Nitta, F. Wu, J. T. Lee, and G. Yushin, "Li-ion battery materials: present and future." *Mater. Today*, **18**, 252 (2015).
4. J. Jaguemont, L. Boulon, and Y. Dubé, "A comprehensive review of lithium-ion batteries used in hybrid and electric vehicles at cold temperatures." *Applied Energy*, **164**, 99 (2016).
5. S. Zhang, K. Xu, and T. Jow, "Charge and discharge characteristics of a commercial licoo2-based 18650 li-ion battery." *Journal of Power Sources*, **160**, 1403 (2006).
6. M. Aneke and M. Wang, "Energy storage technologies and real life applications-a state of the art review." *Applied Energy*, **179**, 350 (2016).
7. J. Jiang and C. Zhang, *Fundamentals and Applications of Lithium-Ion Batteries in Electric Drive Vehicles* (Wiley, Singapore) (2015).
8. T. Chen, Y. Jin, H. Lv, A. Yang, M. Liu, B. Chen, Y. Xie, and Q. Chen, "Applications of lithium-ion batteries in grid-scale energy storage systems." *Transactions of Tianjin University*, **26**, 208 (2020).
9. G. Ning, B. Haran, and B. N. Popov, "Capacity fade study of lithium-ion batteries cycled at high discharge rates." *Journal of Power Sources*, **117**, 160 (2003).
10. R. Kizilel, A. Lateef, R. Sabbah, M. Farid, J. Selman, and S. Al-Hallaj, "Passive control of temperature excursion and uniformity in high-energy li-ion battery packs at high current and ambient temperature." *Journal of Power Sources*, **183**, 370 (2008).
11. Y. Chen and J. W. Evans, "Thermal analysis of lithium-ion batteries." *J. Electrochem. Soc.*, **143**, 2708 (1996).
12. A. M. Aris and B. Shabani, "An experimental study of a lithium ion cell operation at low temperature conditions." *Energy Procedia*, **110**, 128 (2017).
13. K. Amine, J. Liu, and I. Belharouak, "High-temperature storage and cycling of C-LiFePO$_4$/graphite Li-ion cells." *Electrochemistry Communications*, **7**, 669 (2005).
14. J. Hou, M. Yang, D. Wang, and J. Zhang, "Fundamentals and challenges of lithium ion batteries at temperatures between- 40 and 60 °C." *Adv. Energy Mater.*, **10**, 1904152 (2020).
15. M. Safari and C. Delacourt, "Simulation-based analysis of aging phenomena in a commercial graphite and lithium-iron phosphate cell." *J. Electrochem. Soc.*, **158**, A1436 (2011).
16. M. Kassem, J. Bernard, R. Revel, S. Pelissier, F. Duclaud, and C. Delacourt, "Calendar aging of a graphite/LiFePO$_4$ cell." *Journal of Power Sources*, **208**, 296 (2012).
17. W. Choi and A. Manthiram, "Comparison of metal ion dissolutions from lithium ion battery cathodes." *J. Electrochem. Soc.*, **153**, A1760 (2006).
18. H. Yang, G. V. Zhuang, and P. N. Ross Jr, "Thermal stability of LiPF$_6$ salt and li-ion battery electrolytes containing LiPF$_6$." *Journal of Power Sources*, **161**, 573 (2006).
19. S. Ma, H. Lin, L. Yang, Q. Tong, F. Pan, J. Weng, and S. Zheng, "High thermal stability and low impedance polypropylene separator coated with aluminum phosphate." *Electrochimica Acta*, **320**, 134528 (2019).
20. D. P. Finegan et al., "In-operando high-speed tomography of lithium-ion batteries during thermal runaway." *Nat. Commun.*, **6**, 1 (2015).
21. M. Chen, J. Liu, D. Ouyang, and J. Wang, "Experimental investigation on the effect of ambient pressure on thermal runaway and fire behaviors of lithium-ion batteries." *International Journal of Energy Research*, **43**, 4898 (2019).
22. W. Wu, Wei, X. Qiu, and S. Wang, "Low-temperature reversible capacity loss and aging mechanism in lithium-ion batteries for different discharge profiles." *International Journal of Energy Research*, **43**, 243 (2019).
23. D. Ouyang, Y. He, M. Chen, J. Liu, and J. Wang, "Experimental study on the thermal behaviors of lithium-ion batteries under discharge and overcharge conditions." *Journal of Thermal Analysis and Calorimetry*, **132**, 65 (2018).
24. R. Chandrasekaran, "Quantification of bottlenecks to fast charging of lithium-ion-insertion cells for electric vehicles." *Journal of Power Sources*, **271**, 622 (2014).
25. H. Maleki, S. Al Hallaj, J. R. Selman, R. B. Dinwiddie, and H. Wang, "Thermal properties of lithium-ion battery and components." *J. Electrochem. Soc.*, **146**, 947 (1999).
26. M. Koller, J. Unterkofler, G. Glanz, D. Lager, A. Bergmann, and H. Popp, "Radial thermal conductivity measurements of cylindrical lithium-ion batteriesan uncertainty study of the pipe method." *Batteries*, **8**, 16 (2022).
27. S. Saxena, D. Roman, V. Robu, D. Flynn, and M. Pecht, "Battery stress factor ranking for accelerated degradation test planning using machine learning." *Energies*, **14**, 723 (2021).
28. U. Moralı, "Computational modeling and statistical evaluation of thermal behavior of cylindrical lithium-ion battery." *Journal of Energy Storage*, **55**, 105376 (2022).
29. L. Chang, W. Chen, Z. Mao, X. Huang, T. Ren, Y. Zhang, and Z. Cai, "Experimental study on the effect of ambient temperature and discharge rate on the temperature field of prismatic batteries." *Journal of Energy Storage*, **59**, 106577 (2023).
30. X. Xiaoming, J. Fu, H. Jiang, and R. He, "Research on the heat dissipation performance of lithium-ion cell with different operating conditions." *International Journal of Energy Research*, **41**, 1642 (2017).
31. A. Olabi, H. M. Maghrabie, O. H. K. Adhari, E. T. Sayed, B. A. Yousef, T. Salamah, M. Kamil, and M. A. Abdelkareem, "Battery thermal management systems: recent progress and challenges." *International Journal of Thermofluids*, **15**, 100171 (2022).
32. R. Yang, R. Xiong, W. Shen, and X. Lin, "Extreme learning machine-based thermal model for lithium-ion batteries of electric vehicles under external short circuit." *Engineering*, **7**, 395 (2021).
33. W. Du, N. Xue, A. Gupta, A. M. Sastry, J. R. Martins, and W. Shyy, "Optimization of LiMn$_2$O$_4$ electrode properties in a gradient-and surrogate-based framework." *Acta Mechanica Sinica*, **29**, 335 (2013).
34. A. Nazari, S. Kavian, and A. Nazari, "Lithium-ion batteries' energy efficiency prediction using physics-based and state-of-the-art artificial neural network-based models." *Journal of Energy Resources Technology*, **142**, 3 (2020).
35. A. Maheshwari, M. A. Dumitrescu, M. Destro, and M. Santarelli, "A modelling approach to understand charge discharge differences in thermal behaviour in lithium iron phosphate-graphite battery." *Electrochimica Acta*, **243**, 129 (2017).
36. R. Mehta and A. Gupta, "Simulating electrochemical behaviour of lithium-ion cylindrical cells using two-dimensional physics-based model." *Electrochemical Society Meeting Abstracts 237* (Electrochemical Society, Princeton, NJ) p. 323 (2020).
37. D. P. Finegan, J. Zhu, X. Feng, M. Keyser, M. Ulmefors, W. Li, M. Z. Bazant, and S. J. Cooper, "The application of data-driven methods and physics-based learning for improving battery safety." *Joule*, **5**, 316 (2021).
38. P. Khumprom and N. Yodo, "A data-driven predictive prognostic model for lithium-ion batteries based on a deep learning algorithm." *Energies*, **12**, 660 (2019).
39. R. Gupta, R. Mehta, S. S. Bahga, and A. Gupta, "(digital presentation) thermal behaviour prediction of commercial lithium-ion cells under different c-rate and ambient conditions using surrogate modelling." *ECS Meeting Abstracts* (IOP Publishing, Bristol) p. 389 (2022).
40. H. Valladares, T. Li, L. Zhu, H. El-Mounayri, A. M. Hashem, A. E. Abdel-Ghany, and A. Tovar, "Gaussian process-based prognostics of lithium-ion batteries and design optimization of cathode active materials." *Journal of Power Sources*, **528**, 231026 (2022).

41. J. Antony, *Design of Experiments for Engineers and Scientists* (Elsevier, USA) 2nd ed., Chap. 2, p. 7 (2014).
42. F. Pukelsheim, *Optimal Design of Experiments* (SIAM, USA) p. 408 (2006).
43. M. D. McKay, R. J. Beckman, and W. J. Conover, "A comparison of three methods for selecting values of input variables in the analysis of output from a computer code." *Technometrics*, **42**, 55 (2000).
44. F. A. Viana, "A tutorial on latin hypercube design of experiments." *Quality and Reliability Engineering International*, **32**, 1975 (2016).
45. M. Stein, "Large sample properties of simulations using latin hypercube sampling." *Technometrics*, **29**, 143 (1987).
46. N. V. Queipo, R. T. Haftka, W. Shyy, T. Goel, R. Vaidyanathan, and K. Tucker, "Surrogate-based analysis and optimization." *Progress in Aerospace Sciences*, **41**, 1 (2005).
47. N. I. Loonat, A. I. Van Dijk, M. F. Hutchinson, and A. H. Weerts, "Anomaly kriging helps to remove bias in spatial model runoff estimates." *Water Resources Research*, **56**, e2019WR026240 (2020).